JGR Oceans

RESEARCH ARTICLE
10.1029/2022JC019225

Key Points:

- Upslope transport of nutrient is key to fueling nutrients for biological production along the slope and ambient seas
- Interaction between slope current and topography results in strong upslope/downslope nutrient transport along the meandering slope
- Vertical mixing and vertical advection are the major nutrient sources in the upper and lower layer, respectively

Correspondence to:
J. Gan,
magan@ust.hk

Citation:
Lu, Z., & Gan, J. (2023). A modeling study of nutrient transport and dynamics over the northern slope of the South China Sea. *Journal of Geophysical Research: Oceans*, *128*, e2022JC019225. https://doi.org/10.1029/2022JC019225

Received 22 AUG 2022
Accepted 3 MAY 2023

Author Contributions:

Conceptualization: Jianping Gan
Data curation: Zhongming Lu
Formal analysis: Zhongming Lu
Funding acquisition: Zhongming Lu, Jianping Gan
Investigation: Zhongming Lu
Methodology: Zhongming Lu, Jianping Gan
Project Administration: Jianping Gan
Resources: Jianping Gan
Software: Jianping Gan
Supervision: Jianping Gan
Validation: Zhongming Lu, Jianping Gan
Visualization: Zhongming Lu
Writing – original draft: Zhongming Lu
Writing – review & editing: Jianping Gan

A Modeling Study of Nutrient Transport and Dynamics Over the Northern Slope of the South China Sea

Zhongming Lu[1] **and Jianping Gan**[1]

[1]Departments of Ocean Science and Mathematics, Centre for Ocean Research in Hong Kong and Macau, The Hong Kong University of Science and Technology, Kowloon, Hong Kong SAR, China

Abstract Using observed data and results from a numerical model, we investigate the coupled physical-biogeochemical processes that result from water exchanges between the South China Sea (SCS) and the western Pacific Ocean (WPO) and between the shelf and deep basin along the biophysically active continental slope. We study the nutrient transport and dynamics over the northern slope of the SCS where the main branch of the SCS basin circulation facilitates water exchange between the SCS and the WPO. Our results show that the nutrient flux consistently flows year-round into the slope region from the WPO and that the along-slope and cross-slope transports regulate the nutrient budget in the region. The nutrient transport concentrates mainly in the upper 1,000 m and exhibits significant seasonality. We found that cross-isobath motion is key to fueling nutrients for biological production along the slope and throughout the SCS. When the persistent westward slope current interacts with the variable sloping topography, a unique upslope/downslope nutrient transport occurs along convex/concave isobaths. Vertical turbulent mixing becomes the main nutrient source in the upper mixed layer, and vertical advection becomes the major contributor of nutrients to the subsurface layer. Biological production dominates the nutrient sink in both layers. Horizontal advection is also an important sink in winter when the slope current is the strongest due to the enhanced northeasterly monsoon and the Kuroshio intrusion. Our findings provide an insightful understanding on the critical role of nutrient transport over the slope in the overall ecosystem dynamics of the marginal SCS.

Plain Language Summary The transport of the northern continental slope of the South China Sea (SCS) connects the nutrient exchanges not only between western Pacific Ocean (WPO) and the SCS, but also between the shelf and deep basin. Based on a three-dimensional model and observational data, we analyze the exchanges and the underlying biogeochemical processes to illustrate its role on the nutrient budget and ecosystem in the SCS. Our findings indicate that nutrient flow from the WPO to the SCS slope affects the nutrient budget of the SCS (including both the northern shelf and basin). Most nutrient transport is concentrated in the upper 1,000 m with strong seasonality. The upslope cross-isobath nutrient transport is strong due to interaction between slope current and variable slope topography and is key to providing nutrients for the biological production of the SCS. Vertical mixing and vertical advection are the main source of nutrients in the upper mixed layer and the lower layer, respectively. Biological production dominates the nutrient sink in both layers, while horizontal advection is also an important sink when the slope current and intrusion of lower nutrient concentration water from the WPO are strongest.

1. Introduction

The continental slope critically connects a deep ocean basin to the shallow continental shelf and enhanced turbulence found in the region regulates the overall level of mixing in the ocean basin (Gan et al., 2022; Garrett et al., 1993). Although the continental slope occupies a relatively small area, the slope is very important for global climate, biogeochemical cycling, and ecosystem functioning (Heywood et al., 2014). Slope currents exist widely in different parts of the world ocean. These strong currents are trapped against the continental slope and flow along the slope in the direction that a topographic wave would propagate. The along-slope flow generates cross-isobath transport over the sloping bottom topography (Hill, 1995) and results in enhanced exchanges of water, nutrients, and other biogenic elements between the continental shelf and slope.

Physical and biogeochemical processes and dynamics in the slope region in many parts of the world have already been investigated. Numerous field observations, such as the Climate Long-term Interaction of the Mass balance of Antarctica (CLIMA) program and the Antarctic Slope (AnSlope) experiment in the northwest

Ross Sea have enhanced the understanding of the Southern Ocean's shelf-slope exchange (Gordon, Padman, & Bergamasco, 2009). These past studies mainly focused on the slope current and its role in exchanges of mass, heat, and freshwater between the continental shelf and the deep basin (Gordon, Orsi, et al., 2009). For example, Noble and Ramp (2000) analyzed the ocean circulation over the central California slope by deploying moorings to create long-term time series observations. They found that the slope topography strongly constrained variations in the transport. In a different study using hydrographic data captured by ocean gliders, Thompson et al. (2014) revealed that eddy-induced transport is the primary contributor to mass and property fluxes across the Antarctic continental slope and is as important as surface wind-driven transport to the overturning circulation. Combining field observations and numerical modeling, Mizobata et al. (2006) studied the eddy-related cross-slope exchange along the Bering Sea shelf break and demonstrated that mesoscale eddies mainly supply the nutrients that fuel the high biological production at the shelf break.

The South China Sea (SCS) is located to the west of the western Pacific Ocean (WPO) and is one of the largest marginal seas in the world with an area of $\sim 3.5 \times 10^6$ km^2. As a semienclosed marginal sea, the SCS exchanges seawater with the East China Sea (ECS) through Taiwan Strait, with the WPO through Luzon Strait, with the Sulu Sea through Mindoro Strait, and with the Java Sea through the Karimata Strait. The circulation in the SCS is jointly regulated by the East Asian monsoon and the lateral transport through channels connecting adjacent seas (Qu, 2000). The cyclonically and anticyclonically along-slope flow responds to the northeasterly winter monsoon, southwesterly summer monsoon, and the Kuroshio intrusion through Luzon Strait and dominates the basin-scale surface circulation in the SCS (Gan et al., 2006; Gan, Liu, & Hui, 2016; Qu, 2000). The wind force has also been demonstrated to play a very important role in driving cross-isobath transport through wind-driven advection and wind drag effect (Mao & Xia, 2020; Mou et al., 2022). Vertically, a unique three-layer cyclonic-anticyclonic-cyclonic circulation exists in the upper (<750 m), middle (750–1,500 m), and deep (>1,500 m) layers. The inflow-outflow-inflow structure within Luzon Strait and the consequent vortex stretching in the SCS basin produce the unique three-layer alternating circulation (Gan, Liu, & Liang, 2016).

Between the wide shallow northern continental shelf and the deep central basin, the northern slope of the SCS lies between the 200 and 2,000 m isobaths (Liu et al., 2010) and is critical to the physical and biogeochemical processes connecting these two distinct regions. The Kuroshio intrusion and monsoonal wind forcing generate the current over the slope in the northern SCS, and this current shapes the overall SCS basin circulation and controls the SCS throughflow (Gan et al., 2006, 2013; Qu et al., 2006). Kuroshio intrusion through the Luzon Strait greatly affects the northern slope of the SCS, and is one of the most important physical and biogeochemical conditions that regulate the SCS, by the connectivity through the circular slope isobaths. Gan et al. (2022) identified the slope current around the SCS as a dynamic "hot spot" that regulates the three-dimensional circulation and transport in the SCS, and greatly affects the biogeochemical processes in the SCS due to contrasting water properties between the SCS and adjacent western Pacific Ocean (Li & Gan, 2020). Consistent with the depth-dependent characteristic of the slope current, the cross-slope exchange influences ocean circulation and biogeochemical/ecosystem dynamics on the continental shelf and in a deep basin (Thompson et al., 2014). In the SCS, the upslope/downslope motions are key in providing the vertical exchange in the SCS and cannot be completely replaced by mixing (Cai & Gan, 2021; Qu et al., 2006).

Most previous studies in the SCS were conducted on the continental shelf (Gan & Qu, 2008; Gan, Cheung, et al., 2009; Wong et al., 2015) or in the deep basin (Wong et al., 2007; Zhou et al., 2013). However, despite its importance in linking the nutrient flux and the associated biological processes between the shelf and the basin, the fundamental nature of the nutrient transport over the continental slope and the impact of this nutrient transport on the entire ecosystem's dynamics in the SCS are largely unclear. For example, our understanding of the characteristics of current and nutrient transport along the slope, which are coregulated by the adjacent shelf and basin processes, is limited. In addition, we understand little about the upslope intrusion of SCS deep water, the horizontal advection of the intrusive Kuroshio water, and the biogeochemical response to nutrient dynamics and its modulation along the slope (Gan et al., 2022).

In our current study, we use model results to determine the characteristics of the nutrient distribution, transport, and the associated biogeochemical processes that respond to the exchange between the continental shelf and SCS basin. We also determine the characteristics of the local response to the cross-slope transport at the northern slope of the SCS. Our study identifies the key processes governing nutrient transport and dynamics in a typical marginal sea like the SCS.

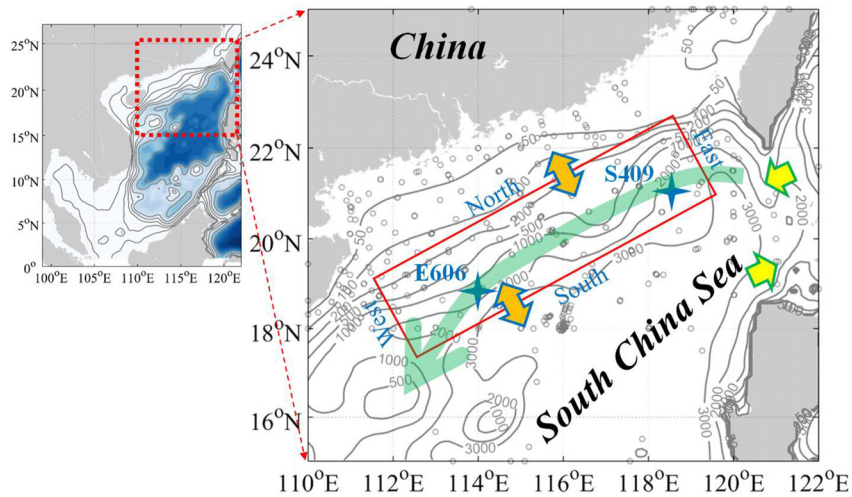

Figure 1. Map with isobaths (m) of the South China Sea (SCS) and an enlargement of the northern slope of the SCS. The red rectangle encloses the slope study area, the four boundaries are marked as North, East, South, and West, respectively. Blue stars show the locations of stations E606 and S409. Gray open circles indicate the stations from various cruises. Yellow arrows with green edges indicate the volume transport through the Luzon Strait. Brown dual-direction arrows with blue edges represent the cross-slope transport. The green arrow represents the annual mean along-slope circulation.

2. Materials and Method

2.1. Observational Data

We used observed field data and remote sensing data to initialize and validate the numerical model. Four cruises under the CHOICE-C project that occurred from July to September 2009, from December 2009 to February 2010, from October to December 2010, and from April to June 2011 provided water column nitrate and phosphate data. For validating the model and subsequent analyses, we only used data from the stations within the slope area (Figure 1). Discrete nitrate and phosphate samples were collected with a Rosette sampler equipped with GO-FLO bottles (General Oceanics Co.), and a flow injection analyzer (Tri-223 autoanalyzer) determined the nutrients colorimetrically. We obtained the monthly remote sensing data from MODIS (Moderate Resolution Imaging Spectroradiometer, averaged from 2002 to 2012) and SeaWiFS (Sea-viewing Wide Field-of-view Sensor, averaged from 1997 to 2010) images. The penetration depth (Z_{pd}) accessible to remote sensing techniques was estimated from the euphotic layer depth (Z_{eu}) and the penetration depth of the blue to blue-green portion of the spectrum. For the model results, we used the mean chlorophyll concentration from the surface to the penetration depth (~22 m in winter and ~29 m during the other seasons) to ensure a reasonable observation-model comparison (Lu et al., 2020).

2.2. Numerical Model and Implementation

Gan, Liu, & Hui (2016) provides details of the physical model and complete model validations, and Gan et al. (2014) provides details of the biological module with governing equations and parameters. The model physics and biogeochemistry were rigorously validated as reported in Gan, Liu, and Hui (2016), Gan, Liu, and Liang (2016), Lu et al. (2020), and Du et al. (2020).

The numerical model we used is the part of China Sea Multi-Scale Ocean Modeling System (CMOMS, https://odmp.ust.hk/cmoms/) that integrates coupled physical-biogeochemical processes at different scales in the China Seas (Gan, Liu, & Hui, 2016; Gan, Liu, & Liang, 2016). CMOMS adopts the Regional Ocean Modeling System (ROMS) (Shchepetkin & McWilliams, 2005) and uses a nitrogen phosphorus colimited biological module that developed on the basis of the ROMS original nitrogen limited biological module (Gan et al., 2014). We added phosphorus, small and large phosphorus detritus to the original model to reflect the P limitation. The stoichiometric relationship between nitrogen and phosphorus in growth, metabolism, and remineralization of phytoplankton, zooplankton, and detritus, was determined according to the Redfield ratio (N:P = 16:1) (Gan et al., 2014). We adopted a curvilinear grid with a (430, 550) dimensional array for the horizontal coordinates (x, y). The horizontal

size of this grid array decreased gradually from ~10 km in the southern part to ~7 km in the northern part of the domain. Vertically, we applied 30-level stretched generalized terrain-following coordinates with higher resolution in the surface and bottom layers. The model domain extended from ~0.95°N, 99°E in the southwest corner to ~50°N, 147°E in the northeast corner.

We forced the model with climatological monthly atmospheric and lateral fluxes (Gan, Liu, & Hui, 2016). The atmospheric heat and salt fluxes were calculated from climatological monthly NCEP (National Centers for Environmental Prediction) reanalysis meteorological variables, and we derived wind stress from the reanalysis 10 m blended sea winds released by the National Oceanic and Atmospheric Administration (https://www.ncdc.noaa.gov/oa/rsad/air-sea/seawinds.html), based on the bulk formulation by Fairall et al. (2003). We initialized the model with winter climatological WOA13 (World Ocean Atlas 2013) salinity and temperature data and forced CMOMS at the boundaries with lateral momentum and buoyancy fluxes from the Ocean General Circulation Model for the Earth Simulator (OFES) global model (Sasaki et al., 2008) and tides from the Pacific Ocean and Indian Ocean subdomains of the Inverse Tide Model (ITM) (Egbert et al., 1994). To integrate the external forcing at the open boundaries, we used a tidal and subtidal (TST) open boundary condition (Liu & Gan, 2016).

For lateral buoyancy fluxes, we used the climatological monthly river discharge from the Information Center of Water Resources (Bureau of Hydrology, Ministry of Water Resource of PR China) and discharge data reported in the literature (Dai & Trenberth, 2002). Based on the literature, and considering the nutrient discharge in organic and/or particulate forms (Duan et al., 2008; Meybeck, 1982), we set the nitrate and phosphate concentrations in the river discharge to be 90 and 1.5 mmol m^{-3}. We merged the initial fields of observed nitrate and phosphate with WOA01 (World Ocean Atlas 2001) data. The WOA01 annual average of chlorophyll provided the initial chlorophyll, and we derived the other biological variables from chlorophyll in fixed proportions (Gan et al., 2014). We also obtained boundary conditions from WOA01.

When calculating annual mean depth-dependent and depth-integrated nutrient fluxes, the model grid is first interpolated to a refined grid with a uniform resolution of 0.01° (~1 km), and then these fluxes are derived from Equations 1 and 2, respectively:

$$N_{yl} = (v_0 \cos\theta - u_0 \sin\theta \cdot [N] \tag{1}$$

$$N_{y2} = \int_{h_0}^{h_1} (v_0 \cos\theta - u_0 \sin\theta) \cdot [N] dz \tag{2}$$

where the subscript, y, represents the direction normal to the isobath; v_0, u_0 are the northward and eastward currents, respectively; θ is the angle between the tangent direction to the isobath and true east; $[N]$ refers to the nutrient concentration; and h_0 and h_1 represent the bottom and surface depths of the integrated layers, respectively.

The angle between the tangential directions of the isobaths is calculated by:

$$\tan\theta_k = \frac{\delta_{y_k}}{\delta_{x_k}}, -\frac{\pi}{2} \le \theta_k \le \frac{\pi}{2}$$

where k is the grid number along the isobaths, δ_{y_k} and δ_{x_k} are defined as $\delta_{y_k} = R(\varnothing_{k+1} - \varnothing_k)$ and $\delta_{x_k} = R(\lambda_{k+1} - \lambda_k)\cos\varnothing_k$, respectively, and R is the radius of the Earth, $\lambda_{k+1} - \lambda_k$ is the longitude difference and $\varnothing_{k+1} - \varnothing_k$ is the latitude difference between the ascending contour points (Gan, Li, et al., 2009).

3. Modeled and Observed Characteristics

We examined the vertical structure of the nutrients of the northern continental slope of the SCS by comparing the simulated model results with the observed data from the four cruises. To evaluate the biological response, we compared the horizontal distribution and time series variation of the surface chlorophyll with the satellite remote sensing data.

3.1. Vertical Nutrient Distribution

The WPO intrusive current through Luzon Strait and the Southeast Asian monsoon mainly shape the circulation over the northern slope of the SCS (Gan et al., 2006). The flow over the slope, or slope current, dominates the

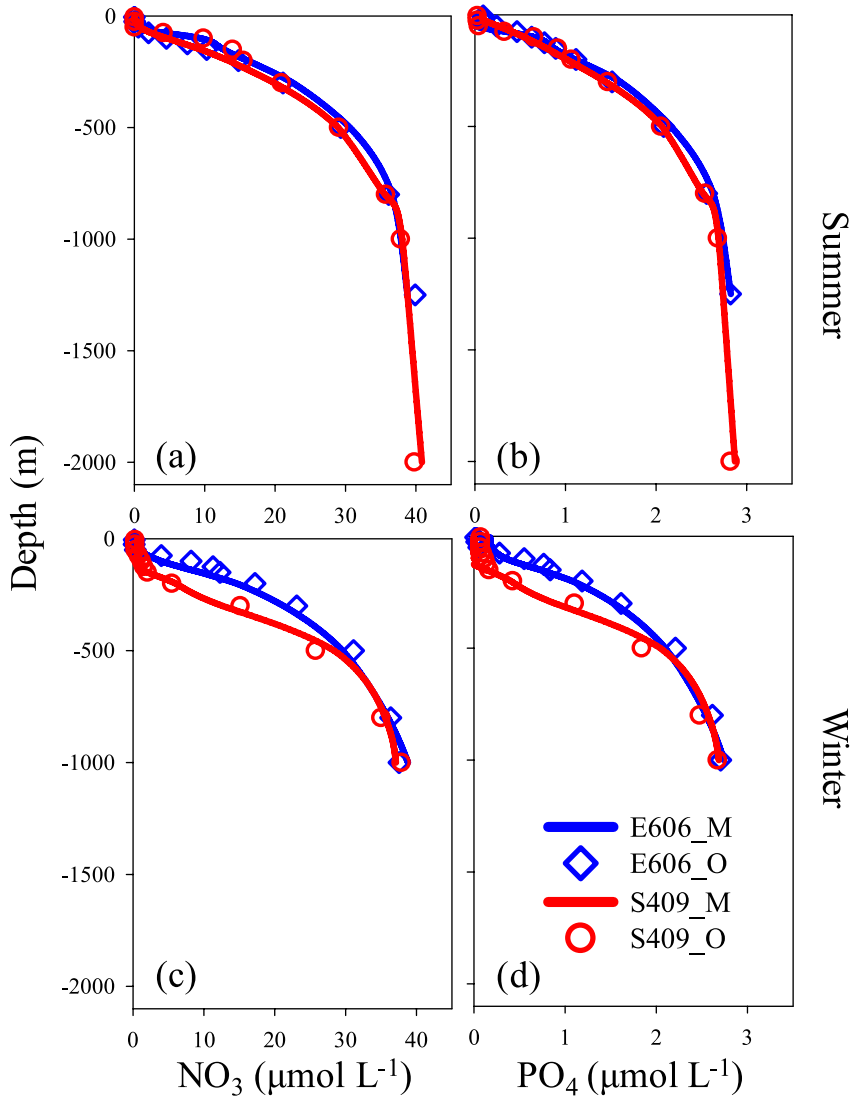

Figure 2. Vertical profiles of (a, c) NO_3 and (b, d) PO_4 from the model results and field observations at E606 and S409 stations (see Figure 1 for locations) in summer (upper panel) and (lower panel) winter. Blue solid lines represent model results at E606. Blue open diamonds represent observations at E606. Red solid lines represent model results at S409. Red open circles represent observations at S409.

water transport in the basin (Gan, Liu, & Hui, 2016; Qu, 2000). The monsoonal wind and the Kuroshio intrusion force the basin-scale cyclonic circulation that forms a constant southwestward current in the upper layer along the northern slope of the SCS (Gan, Liu, & Liang, 2016). When the intrusive Kuroshio water and the SCS water interact, the water properties of the region change.

Figure 2 shows the vertical profiles of NO_3 and PO_4 at stations S409 and E606, representing upstream and downstream locations of the slope current, respectively. The model results agree with the observed vertical profiles reasonably well for both stations and across all seasons. In summer, the vertical distributions of nutrients at these two stations are similar (Figures 2a and 2b). However, there are significant disparities in the nutrient distributions between the two stations in the upper layer during winter. The nutrient concentration at S409 is considerably lower than at E606 in the upper ~600 m, except in the upper mixed layer where the nutrients are nearly depleted due to biological consumption. The maximum differences are as high as 12 and 0.8 μmol L^{-1} for NO_3 and PO_4, respectively, at ~200 m (Figures 2c and 2d). The winter difference occurs because of the stronger Kuroshio intrusion during winter (Gan, Liu, & Hui, 2016) and the huge winter difference in nutrient concentration between the SCS and the WPO (Du et al., 2013; Gong et al., 1992, Lu et al., 2020).

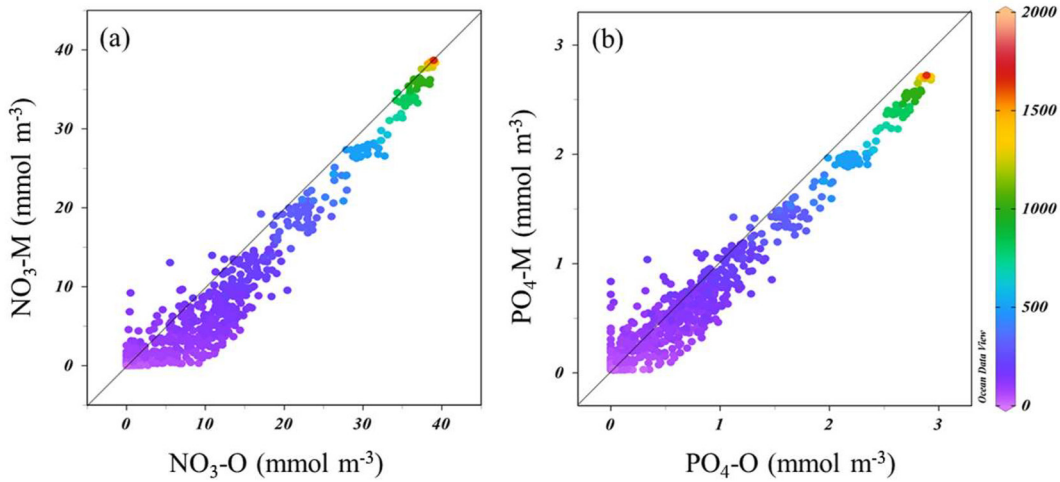

Figure 3. Comparison between model (M) and observations (O) for (a) NO_3 and (b) PO_4. Each point in the scatter charts represents an observation-model pair The observational data used in this figure were collected from the stations enclosed by the red rectangle in Figure 1. The color of the points represents the sampling depth of each data point.

We also compared the model results and observations at all the sampling stations from the various cruises in the study area (Figure 3). In general, the model results maintain a 1:1 relationship with the observed data, but there is a slight systematic bias, especially in the upper layer where biogeochemical activities are relatively strong. The deviation probably due to a mismatch between the simulation and observation periods. Nevertheless, there is good overall linearity between the model results and the observations, demonstrating that the model captures the observed features reasonably well for the northern slope of the SCS.

3.2. Distribution of Surface Chlorophyll

The summer and winter horizontal distributions of the surface chlorophyll vary significantly spatiotemporally (Figures 4a–4d). This variability is also present in the time series of the domain-averaged surface chlorophyll of the model results and satellite remote sensing data (Figure 4e). The water column in the region is well-stratified during most of the year due to the intrusion of warm Kuroshio water and because the surface water is insulated from the deep water by a stable pycnocline (Gan, Liu, & Hui, 2016).

In summer, nutrients are nearly depleted in the mixed layer (Wu et al., 2003), and the surface chlorophyll level is low (<0.2 μg L^{-1}) (Figures 4a and 4c). In addition, the chlorophyll level in the surface layer is very low in spring and autumn for similar reasons. A relatively high level of chlorophyll (0.2–0.5 μg L^{-1}) only occurs during the winter when the strong northeasterly monsoon stirs the water. The wind favors upward mixing of nutrients from the subsurface layer, which stimulates phytoplankton growth in the surface layer (Figures 4b and 4d). Additionally, an area of high chlorophyll around Dongsha Island throughout the year occurs in the observations and the simulated results (Figures 4a–4d). Li et al. (2015) suggested that the enhanced surface chlorophyll in this region is probably due to increased vertical mixing by the cyclonic and anticyclonic eddies distributed southwest and southeast of Dongsha Island. The stronger diapycnal diffusivity near the island due to the internal tide propagating westward from Luzon Strait might also increase the surface nutrient concentration and enhance the surface chlorophyll level. Strong fronts due to Kuroshio intrusion and interactions with the SCS water may also lead to strong phytoplankton growth in this region (Guo et al., 2017).

Figure 4e shows the time series of the domain-averaged surface chlorophyll levels of the model output and the field observations. The chlorophyll level reaches its annual maximum (~0.33 μg L^{-1}) in January, reflecting the high nutrient concentration due to strong vertical mixing. Otherwise, the chlorophyll level remains relatively low (~0.11 μg L^{-1}) for most of the year (April to November), reflecting oligotrophy in this area. The model reasonably reproduces the spatial variability and seasonality of the biological response in the northern slope region of the SCS.

The simulated spatiotemporal characteristics of the nutrients and chlorophyll agree with our general understanding of the biogeochemical processes in the SCS. However, the controlling mechanisms have yet to be systematically assessed. To elucidate the internal regulatory factors/processes, we focus on the influence of the water

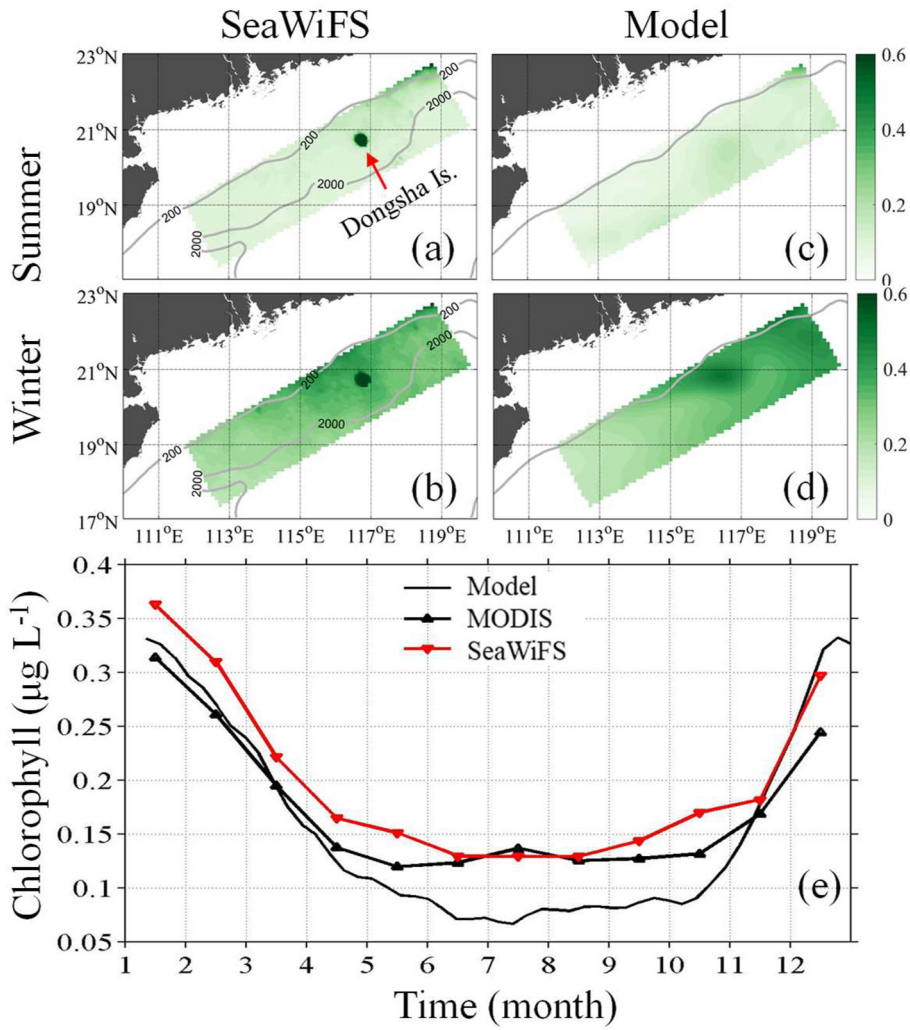

Figure 4. Horizontal distribution of sea surface chlorophyll (μg L^{-1}) in summer and winter from (a, b) SeaWiFS satellite data and (c, d) model results. (e) Seasonal variation in domain-averaged sea surface chlorophyll from the model and MODIS and SeaWiFS.

exchange through boundaries of the slope area and the upslope/downslope motions of the nutrient transport, dynamics, and biological responses in the region.

4. Nutrient Flux, Transport, and Dynamics

The strong current and kinetic energy of the northern slope of the SCS (Gan et al., 2022) shape the three-dimensional transport of biogeochemical substances, and the along-slope current connects the northern and southern basins while the cross-slope currents link the shelf and the basin. Understanding the processes that govern the transport are crucial to depicting the biogeochemical dynamics of the northern slope of the SCS and in the shelf and basin of the SCS. The key governing processes include the nutrient flux into/out of the northern slope region, the upslope/downslope nutrient transport, and the nutrient dynamics and biological feedback in the upper layer.

4.1. Cross-Boundary Nutrient Transport

The Southeast Asian monsoon drives the slope current over the northern slope of the SCS, and the Kuroshio intrusion from the WPO through Luzon Strait modulates the current (Gan et al., 2006; Gan, Liu, & Hui, 2016). Strong influxes (flow into the slope zone) of nutrients through the eastern boundary are simulated in the annual means shown in Figure 5a (represented by the nitrate flux). The transport in Luzon Strait has an inflow-outflow-inflow sandwich structure in the upper-middle-deep layers, respectively (Gan, Liu, & Liang, 2016). Yet, the nutrient flux

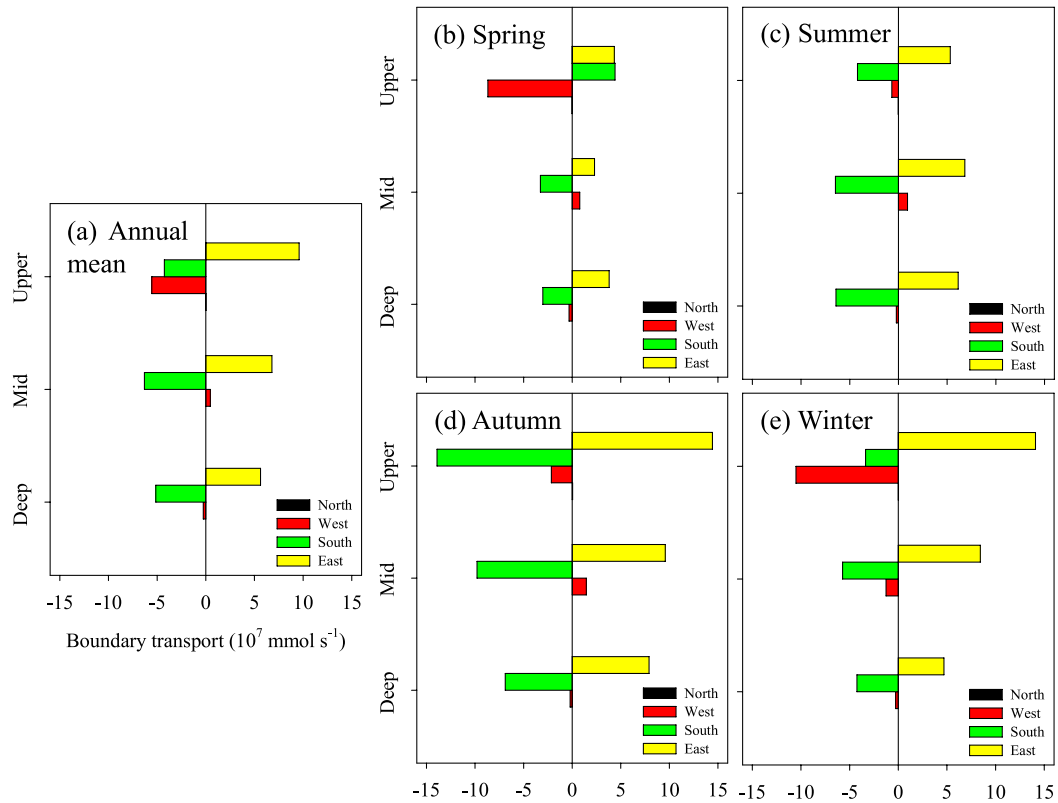

Figure 5. Domain and layer-integrated simulated nitrate flux through the north, west, south, and east boundaries in the upper (<750 m), middle (750–1,500 m), and deep (>1,500 m) layers of the northern slope of the SCS for (a) annual mean, (b) spring, (c) summer, (d) autumn, and (e) winter. Positive/negative values represent nitrate flow into/out of the domain.

through the eastern boundary of our study region has inflow in all three layers in different seasons (Figure 5). This complete inflow is because the eastern boundary of the northern slope of the SCS is directly in the path of the Kuroshio intrusion current. The intrusion of the Kuroshio through Luzon Strait is mainly located in the north part of the strait (south of Taiwan), and the outflow is mainly in the south part of the strait (north of Luzon Island, Philippines; Figure 1) (Li & Gan, 2020). Therefore, the outflow and export of nutrients through Luzon Strait occurs mainly on the seaward side of the slope in the deep basin.

After intruding onto the northern slope of the SCS region, the current flows along the steep slope around the basin and forms the basin-wide slope circulation (Gan et al., 2006). In the upper layer, the main portion of the slope current flows off the northern slope of the SCS along the west continental margin while a smaller portion flows southwesterly off the northern slope. The former portion eventually flows out of the SCS through Karimata Strait, and the latter portion exits the SCS through Mindoro Strait. Together, the two portions form the SCS throughflow (Qu et al., 2009).

The nutrient flux crossing the northern boundary has a much smaller magnitude than the transports through the eastern and western boundaries (Figure 5) due to the shallower water in the north, the oligotrophic waters of the northern region (Wu et al., 2003), and the relatively weak cross-slope current in the north. Quantitative analysis will be performed in the next section.

The nutrient transport across the different boundaries is also strongly seasonal (Figure 5). The overall transport through the eastern boundary is stronger in autumn and winter when the westward intrusion of the Kuroshio is stronger because the Kuroshio Current is weaker in this period (Qu, 2000). Unlike at the eastern boundary, the western boundary is much farther from Luzon Strait and the nitrate flux through the western boundary appears to be affected more by the cyclonic-anticyclonic-cyclonic circulation in the upper, middle, and deep layers, respectively, with differing seasonality (Gan, Liu, & Liang, 2016) governing the slope current in the region (Cai & Gan, 2021; Gan et al., 2022). Nutrient outfluxes through the western boundary occur mainly in the upper layer and concentrate mainly in autumn and winter, reflecting the stronger slope current due to an intensified

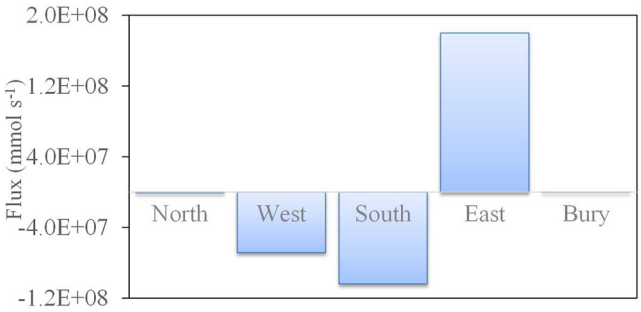

Figure 6. Simulated annual mean nitrogen flux through northern, western, southern, and eastern boundary. The nitrogen flux includes NO_3, NH_4, phytoplankton, zooplankton, large detritus, and small detritus, and the bury include phytoplankton, large detritus and small detritus. Positive/negative values represent nitrate sources/sinks of the region.

northeasterly monsoon and Kuroshio intrusion through Luzon Strait. Opposite to the seasonal variations of the transport through the eastern and western boundaries, the nutrient transport through the southern boundary is stronger in summer and autumn as a result of the weaker along-slope current. The nutrient is transported onshore (-0.020×10^7 mmol s^{-1} in upper layer, the transport is close to 0 in midlayer and deep layer) through the northern boundary in summer and offshore (0.025×10^7 mmol s^{-1} influx) in winter. The nutrient transport through northern boundary is orders of magnitude lower than that through eastern and southern boundaries, so that it cannot be distinguished in the figure (Figures 5c and 5e).

Figure 6 shows the annual mean nitrogen budget of the northern slope region depicted by the inset box in Figure 1. The eastern boundary input into this region is clearly the main source of nitrogen (annual mean = 1.8×10^8 mmol s^{-1}). The outflows through the western and southern boundaries are almost equally important sinks (-6.8×10^7 and -1.1×10^8 mmol s^{-1}, respectively). The contribution from the nitrogen buried in the sediment is minor in this region compared to the entire SCS (Chen et al., 2001) due to the deep water and relatively small area of the northern slope.

4.2. Upslope and Downslope Nutrient Transport

Except for the year-round southwestward transport due to Kuroshio intrusion across the eastern boundary, there is significant seasonal and vertical variability in the cross-slope transport through the other boundaries (Figure 5 in Section 4.1), likely due to the spatiotemporal variation in the slope current affected by the Luzon Strait inflow/outflow and the monsoonal wind (Gan et al., 2006). The cross-slope transport is highly variable and intermittent in time and space (Gordon et al., 2004; Mizobata et al., 2006) also due to the variable slope topography.

To illustrate how the cross-isobath transport forms at different locations along the slope, we calculated the cross-isobath nutrient fluxes along the 200, 500, 1,000, and 2,000 m isobaths of the northern slope of the SCS (Figure 7). We obtained the annual mean depth-dependent (Figures 7a–7d) and depth-integrated (Figure 7e) nitrate fluxes from Equations 1 and 2, respectively.

In the lower layer, the cross-slope flux of nutrients does not follow the same pattern as the velocity in the upper layer (especially the top ~100 m) due to the rapidly changing nutrient concentration in the upper 750 m (Figure 2). The core of the nutrient upslope/downslope flux rises from ~600 m (upper layer) on the basin side (2,000 m isobath, Figure 7d) to ~150 m (bottom layer) on the shelf side (200 m isobath, Figure 7a). Unlike the episodically occurring cross-slope transport over the continental slope of the Arctic Ocean and the Antarctic Ocean (Gordon et al., 2004; Mizobata et al., 2006), there are strong and persistent cross-isobath nutrient fluxes over the northern slope of the SCS. The cross-isobath nutrient fluxes vary in magnitude and direction along the slope, exhibiting a unique alternating distribution along the slope. The upslope/downslope transport is unique in the sense that it is jointly regulated (forced) by the wind forcing above, Kruoshio intrusion from the east and from the interior of the South China Sea over the alternative broad convex/concave slope isobaths. The pathways for the nutrient cross-slope exchange are spatially fixed along the northern slope of the SCS (Figure 7e), indicating the control that the topography has on the flow. Figures 7a–7e show that the strongest upslope transport occurs on the easternmost side of the northern slope of the SCS where the curvature of the shoreward convex isobaths attains its maximum. At the same time, the strongest downslope transport occurs on the western side over the shoreward concave isobaths. Similar pathways of the upslope/downslope transport also occur at the neighboring convex/concave isobaths, resulting in the alternating distribution of the upslope/downslope pathways. The along-slope variable sea surface elevation and the along-isobath pressure gradient force associated with the bottom topography are the controlling factors of the variable cross-slope transport (Gan & Allen, 2002; Gan, Li, et al., 2009). As indicated by the vertical profile of the cross-slope nitrate flux (Figures 7a–7d), the cross-isobath exchange weakens as the water depth decreases and as the strength of the slope current weakens.

By integrating the upslope and downslope transports over the entire water column, we obtained the variations of the cross-slope nitrate transport with depth in the shoreward and seaward directions, respectively (Figure 7f). We see that the shoreward transport is generally stronger from the 200 m to the 2,000 m isobath over the slope. Although

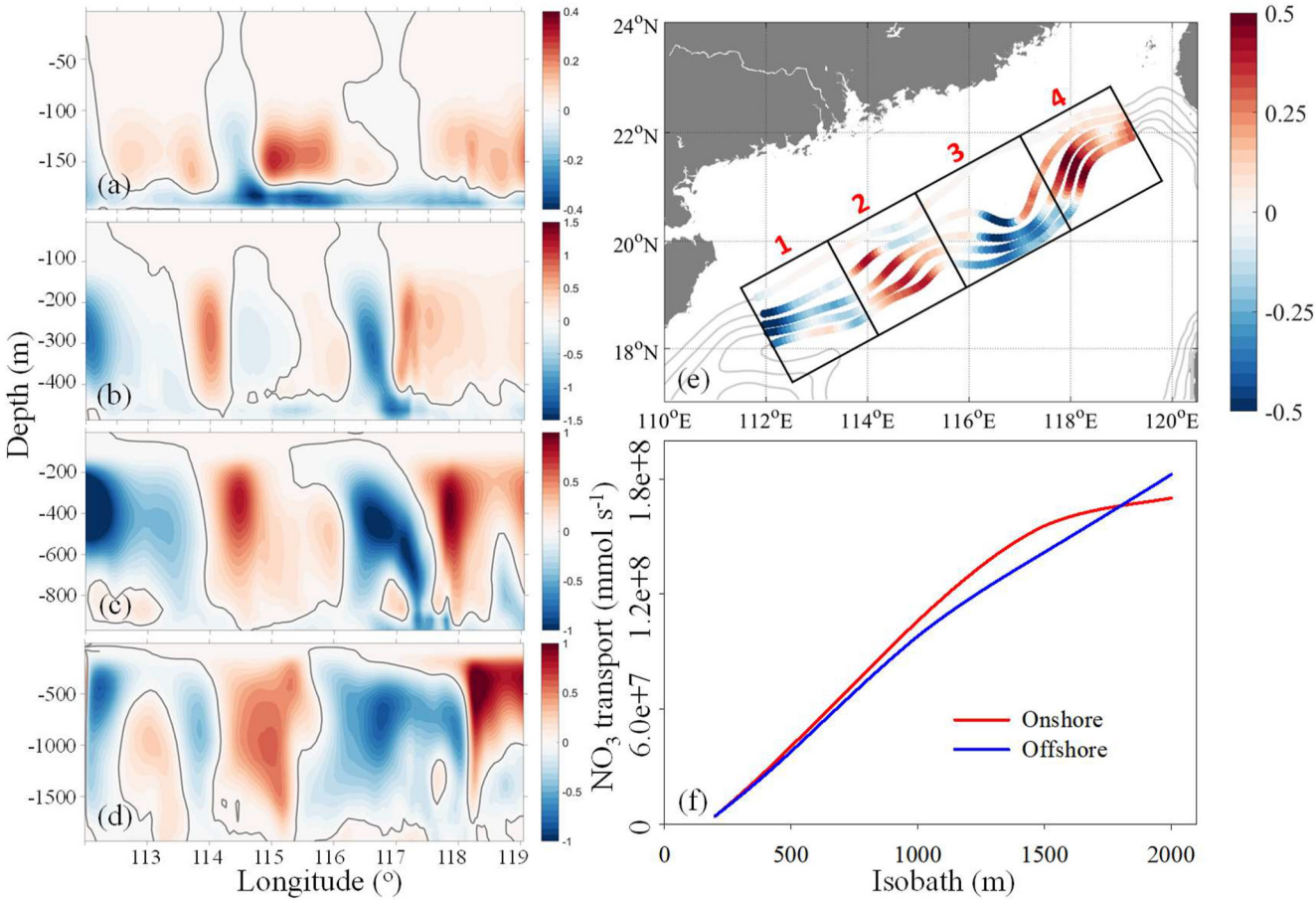

Figure 7. Simulated vertical distributions of annual-mean cross-slope nitrate flux (mmol m^{-2} s^{-1}) along (a) 200 m, (b) 500 m, (c) 1,000 m, and (d) 2,000 m isobaths. The gray contour represents 0 value. (e) Simulated depth averaged annual-mean cross-slope nitrate flux (mmol m^{-1} s^{-1}) along the 200 m, 500 m, 1,000 m, 1,500 m, 2,000 m isobaths. Black boxes marked with 1, 2, 3, and 4 are alternative convex and concave zones over the slope to be discussed in Figure 8. Positive/negative values in (a– e) represent onshore/offshore flux. (f) Simulated annual-mean depth-integrated onshore (red solid line) and offshore (blue solid line) transport of nitrate (mmol s^{-1}) for the whole domain, indicating cross-slope exchange of nitrate flux.

the transport across the 200 m isobath connecting the shelf and slope (~2.4×10^6 mmol s^{-1}, or ~6 mmol m^{-1} s^{-1}) is relatively small compared with the transport across deeper isobaths (~2% of the transport across the 2,000 m isobath), it is still about four times larger than the terrestrial nutrient input from the largest river in this region (Lu et al., 2018). The amount of nutrients provided by the cross-slope transport is a rich nutrient source that is transported shoreward at a rate of ~2 mmol m^{-1} s^{-1} NO_3 across the 50 m isobath with the coastal upwelling (Gan et al., 2010).

By dividing the alternating upslope/downslope transport along the convex/concave topography over the slope, we see there are four major pathways (or zones) over the northern slope (Figure 7e) where the downslope transport occurs in Zones 1 and 3, and the upslope transport occurs in Zones 2 and 4. By horizontally averaging the cross-slope nitrate transport in the four zones, we obtained the vertical profiles of nitrate transport in this region for different seasons shown in Figure 8. The upslope and downslope transports are significantly stronger in summer than in winter, consistent with the cross-boundary transport discussed in Section 4.1. The seasonal variations in the net transport are relatively small. In the upper 500 m, nitrate is transported shoreward in summer and winter. Spring and autumn exhibit short transient features between winter and summer and between summer and winter, respectively. To avoid distractions, we focused on analyzing the characteristics in summer and winter.

4.3. Water Column Nutrient Dynamics

A strong cyclonic current along the sloping topography and the alternating upslope/downslope transport enhance nutrient exchanges with the adjacent shelf and basin. The response and feedback of the biological activities in the

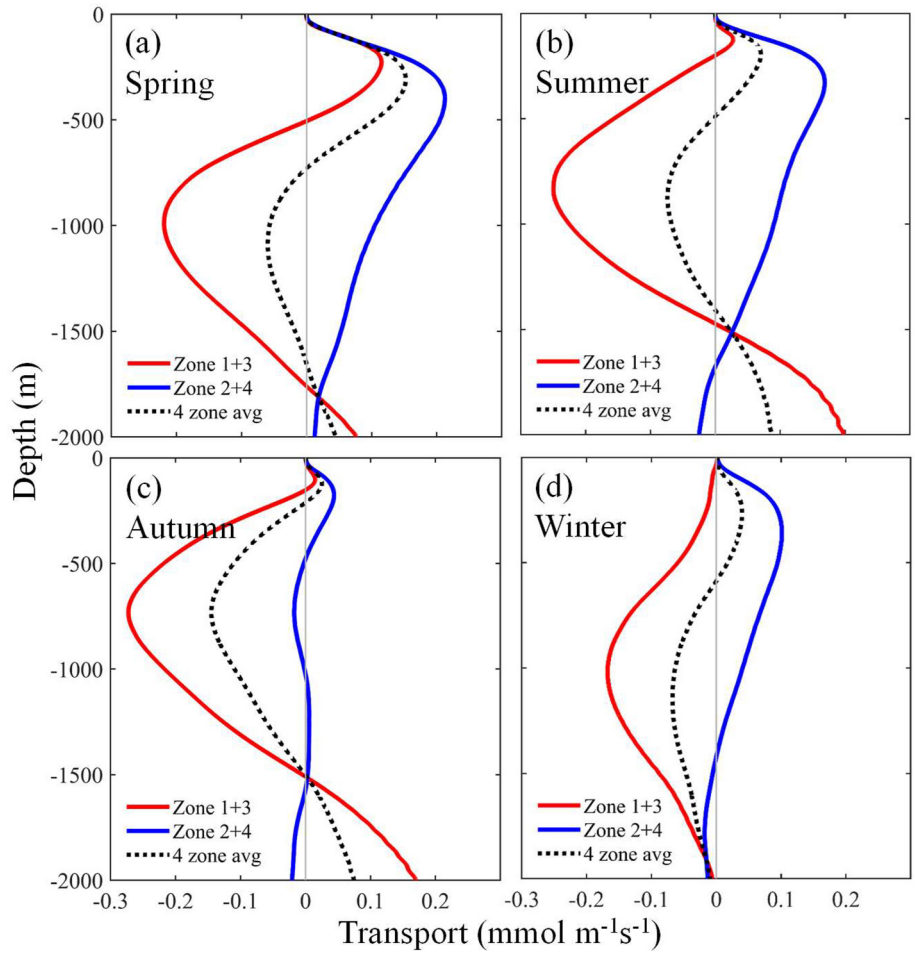

Figure 8. Simulated horizontally averaged cross-slope NO_3 transport for Zones 1 to 4 (refer to Figure 7 for location) during (a) spring, (b) summer, (c) autumn, and (d) winter.

upper layer further complicate the nutrient dynamics because of assimilation and remineralization which intensify the vertical gradient and accelerate vertical transport over the slope. To determine how the different processes affect the variation in nutrients and to conduct a first-order assessment of the nutrient dynamics, we calculated the time series of the volume-averaged nitrate in the different layers of the northern slope based on nitrate's governing equation in the model (Equation 3):

$$\frac{\partial [N]}{\partial t} = A[N] + D[N] - \mu_{\max} f(I)[Phyto]\left[\frac{\sigma_N \frac{[N]}{K_N+[N]} \cdot \frac{1}{1+\frac{[A]}{K_A}} +}{\sigma_P \cdot \frac{[N]}{[N]+[A]} \cdot \frac{[P]}{K_P+[P]}}\right] + n[A] \quad (3)$$

where $A[N]$ and $D[N]$ are advection and diffusion terms of nitrate. N, A, P, and $Phyto$ represent NO_3, NH_4, PO_4, and phytoplankton, respectively. $\mu_{\max}$ is the maximum growth rate of phytoplankton at a given temperature T (Eppley, 1972). $f(I)$ represents the photosynthesis-light (P-I) relationship. σ_N and σ_P are nutrient limitation coefficients where $\sigma_N = 1$ and $\sigma_P = 0$ when N is limited and $\sigma_N = 0$ and $\sigma_P = 1$, otherwise. k_N, k_A, and K_P are half-saturation constants for phytoplankton uptake by NO_3, NH_4, and PO_4, respectively, and n is the nitrification rate that is regulated by light (Olson, 1981).

As shown by the transport through the boundaries in Figure 5 and the cross-isobath fluxes in Figure 7, the nutrient transport is mostly concentrated in the upper layer, mainly due to the stronger intrusion through Luzon Strait and the effects of wind forcing (Gan, Liu, & Liang, 2016). The concentrated nutrient transport is also caused by the "insulating effect" on the steep slope due to the bottom stress curl and vortex stretching over the slope (Csanady

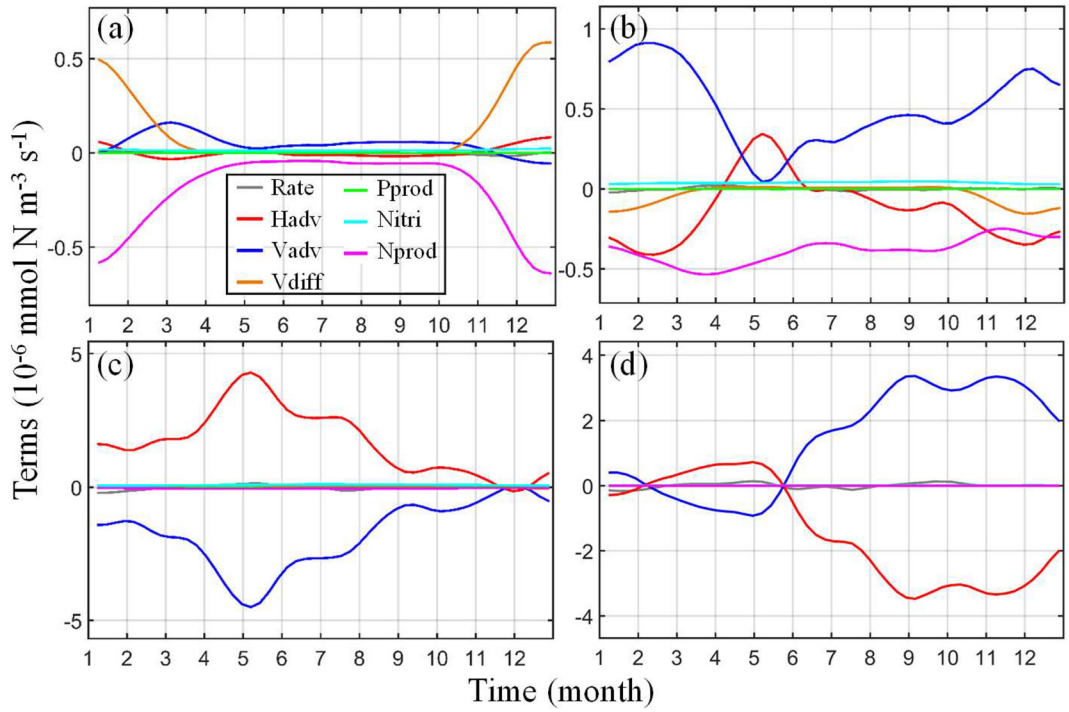

Figure 9. Time series of volume-averaged terms in the NO_3 equation in the (a) 20 m, (b) 20–50 m, (c) 50–200 m, and (d) 200–500 m averaged in the water column over the northern slope of the SCS. All terms are calculated by placing them on the right side of the equation, such that a negative rate means an increasing rate of variation and a positive rate means a decreasing rate of variation. Hadv = horizontal advection, Vadv = vertical advection, Vdiff = vertical diffusion, Pprod = production by PO_4, Nitri = nitrification, Nprod = production by NO_3.

& Shaw, 1983). For these reasons, we focus our analysis of nutrient dynamics over the northern slope in the upper 500 m.

The SCS is an oligotrophic marginal sea (Wu et al., 2003), the nutrient concentration in the upper mixed layer (upper 20 m (Qu, 2001; Qu et al., 2007) is generally below the detection limit of conventional detection methods, except in winter when the prevailing northeastern monsoon is strong. In winter, the major nutrient source term is vertical diffusion (or turbulent mixing) while the major sink is biological uptake, indicated by NProd in Figure 9a. In the figure, Pprod and Nprod can reflect the relative proportion of P-limited area and N-limited area. As we known, the surface water of the SCS is generally N-limited, therefore we can find that the green line (represent Pprod) is basically zero. All the sources and sinks in this layer (upper 20 m) are weak during other seasons when wind stirring and cooling convection subside (Qu et al., 2007). In the subsurface layer (20–50 m), where turbulent mixing is much weaker, but the nutrient concentration is still very low, vertical advection across the top of the nutricline at ~50 m depth (Wong et al., 2002) is the dominant nutrient source (Figure 9b). In the SCS, the plankton biomass is concentrated in the subsurface layer for most of the year, because of adequate photosynthetically active radiation (PAR) and sufficient nutrient supply from nutricline (Lu et al., 2010). As a result, biological uptake acts as the most important nutrient sink throughout the year (Figure 9b). Horizontal advection also serves as a sink for the nutrients because of dilution (Lu et al., 2020), especially during winter when the westward WPO intrusion through Luzon Strait is strong (Gan, Liu, & Hui, 2016). NO_3 is mainly sourced from vertical advection. Horizontal advection is a source only during a short period in late spring probably due to local cyclonic eddies (Gan et al., 2006). The horizontal convection carries water with higher nutrient concentration into the slope region through the southern boundary (Figure 5). Nutrient transport by cyclonic eddies (Cai & Gan, 2020) reaches its maximum in the 50–200 m layer (Figure 9c) and can penetrate to the 200–500 m layer (Figure 9d). In the upper nutricline between ~50 and ~500 m (Wong et al., 2002), the nutrient concentration increases rapidly as biological activities decrease, and horizontal and vertical advection alternate in dominating the source and sink terms (Figures 9c and 9d). The advection terms are also the strongest because the strongest slope currents are located within this upper nutricline layer. The extremely strong nutrient contribution from

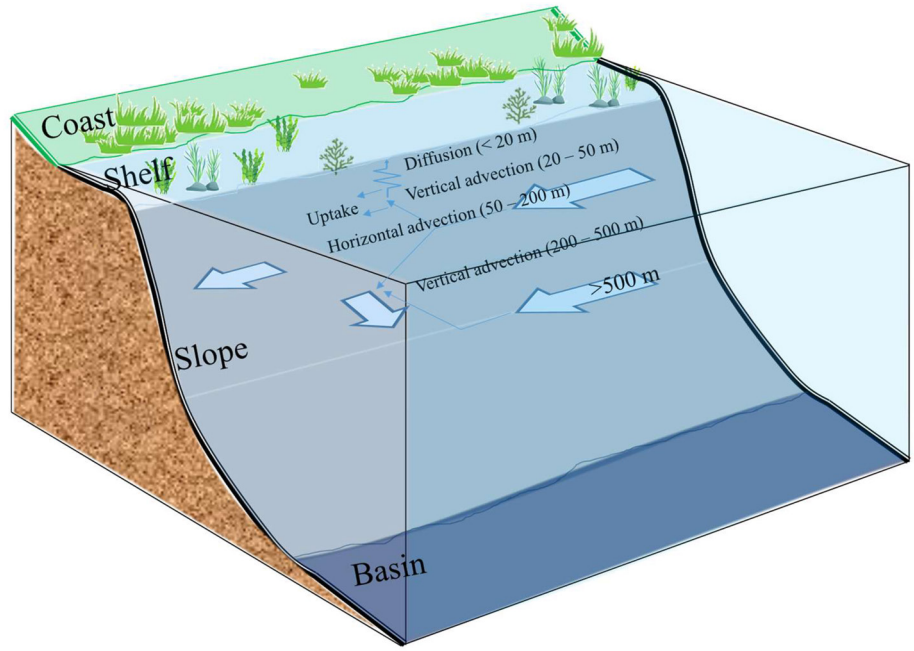

Figure 10. Schematic illustration of nutrient dynamics over the northern slope of the South China Sea (SCS).

advection distinguishes the nutrient dynamics on the northern slope of the SCS from those on the SCS shelf and basin (Lu et al., 2020), reflecting the effect of the unique slope circulation.

Figure 10 summarizes the nutrient dynamics in the upper layer (upper 500 m) of the northern slope. For the whole region, nutrients are mainly sourced from lateral horizontal advection between 50 and 200 m and from upward advection through the 500 m layer. Vertical advection of a portion of the nutrients flowing within the 50–200 m layer replenishes the nutrient-depleted subsurface layer. Vertical diffusion helps these nutrients to eventually reach the upper mixed layer and support new production where phytoplankton consume the nutrients. Eventually, these nutrients are from this mixed layer when the phytoplankton die and sink. Another portion of the nutrients moves downward and unites with the upward flowing nutrient supply from the deeper layer (>500 m) before the nutrients flow out of the northern slope region because of horizontal advection. If the nutrient transport is integrated across the entire upper 500 m of the water column, the horizontal advection becomes the major nutrient sink because of dilution (Lu et al., 2020), and the vertical advection becomes the major source of nutrients in the region. Below the top of the nutricline the biological effects on the nutrients are relatively weak compared to the effects of advection. Our results demonstrate the joint control of physical and biological effects on the nutrient content in the region.

5. Summary

This study combined observed data with coupled physical-biogeochemical simulations from CMOMS to identify characteristics of spatiotemporal nutrient distribution, quantify nutrient transport and budget and investigate underlying dynamics over the northern slope of the SCS. We found that active nutrient exchange and variability along meandering slope played critical role in governing nutrient transport and distribution in the SCS.

The Kuroshio intrusion and the Southeast Asian monsoon shape the influx of nutrients into the northern slope. The influx is stronger in winter when the Kuroshio westward intrusion strengthens due to the weakened Kuroshio current. Nutrients exit the northern slope and transport southwestward along the slope through the western boundary and seaward into the SCS basin through the southern boundary of the slope. There is a relatively weak landward transport, which, however, plays an important role in supplying nutrient deep slope water and regulating biological activities on the northern continental shelf. The nutrient cross-slope transport core locates at the depths ranging from ~600 to ~150 m where the slope current is the strongest. The alternative shoreward/seaward transport occurs along the convex/concave slope.

We quantified physical and biological processes that control nutrient budget in different layers over the northern slope. In the upper mixed layer, sources and sinks of nutrient are weak except in winter when wind stirring mixing and cooling convection strengthen. Vertical diffusion is the major source of nitrate, and biological uptake is the major sink. In the subsurface layer, vertical advection replaces diffusion as the dominant nutrient source, with biological uptake remaining the major sink. Horizontal advection in the upper layer is only a sink in winter when the nutrient-depleted Kuroshio intrusion is strong. In the deeper layer, horizontal and vertical advection alternate as source and sink due to variable slope current, cyclonic eddies, and vertical nutrient distribution. Strong slope current and the associated cross-slope transport form the active region for nutrient exchange vertically and horizontally in the SCS.

It should be noted that the effect of submesoscale processes may affect the mixing and high-mode processes of both physical and biogeochemical processes in the region. Although they may have limited effect on the mainly mesoscale transports discussed in this study, their effect in the SCS and global ocean need to be further investigated. Using climatological forcing, this study successfully identified the dominant characteristics of nutrient distribution, transport, budget, and underlying complex coupled physical-biogeochemical dynamics over the slope, which laid a solid foundation for the future study of much complex dynamics under higher-frequency atmospheric forcing and with time-dependent biogeochemical parameters. This study sheds light on the critical role of slope circulation as a major 3D conveyor for momentum and biogeochemical substances in the marginal SCS.

Data Availability Statement

The MODIS data are available at NASA Goddard Space Flight Center et al. (2018) via the http://doi.org/10.5067/AQUA/MODIS/L3M/CHL/2018; The SeaWiFS data are available at SeaWiFS Mission page (2019) via the http://doi.org/10.5067/ORBVIEW-2/SEAWIFS/L2/OC/2018. All the numerical information was produced by solving equations in the Regional Ocean Modeling System (ROMS) (Shchepetkin & McWilliams, 2005). The source code for ROMS is available at https://www.myroms.org/; The model data for this study are available at https://odmp.ust.hk/cmoms/; The results used in the study are on the web site https://ocean.hkust.edu.hk/data/?page_id=693.

Acknowledgments
This research was supported by Key Project of the National Science Foundation of China (41930539), the Hong Kong Research Grants Council (GRF 16308319) and the Hong Kong Research Grants Council Theme-based Research Scheme (T21-602/16-R). Center for Ocean Research in Hong Kong and Macau is jointly established by Qingdao National Lab of Marine Science and Technology and The Hong Kong University of Science and Technology. We thank Mr. Xiaozhen Zhao for his help with the data processing. We are also grateful for the support of The National Supercomputing Center of Tianjin and Guangzhou.

References

Cai, Z., & Gan, J. (2020). Dynamics of the cross-layer exchange for the layered circulation in the South China Sea. *Journal of Geophysical Research: Oceans*, *124*, e2020JC016131. https://doi.org/10.1029/2020JC016131

Cai, Z., & Gan, J. (2021). Dynamics of the layered circulation inferred from kinetic energy pathway in the South China Sea. *Journal of Physical Oceanography*, *51*(5), 1671–1685. https://doi.org/10.1175/JPO-D-20-0226.1

Chen, C. T. A., Wang, S. L., Wang, B. J., & Pai, S. C. (2001). Nutrient budgets for the South China sea basin. *Marine Chemistry*, *75*(4), 281–300. https://doi.org/10.1016/s0304-4203(01)00041-x

Csanady, G. T., & Shaw, P. T. (1983). The insulating effect of a steep continental-slope. *Journal of Geophysical Research: Oceans*, *88*, 7519–7524. https://doi.org/10.1029/JC088iC12p07519

Dai, A., & Trenberth, K. E. (2002). Estimates of freshwater discharge from continents: Latitudinal and seasonal variations. *Journal of Hydrometeorology*, *3*(6), 660–687. https://doi.org/10.1175/1525-7541(2002)003<0660:EOFDFC>2.0.CO;2

Du, C., Gan, J., Hui, C. R., Lu, Z., Zhao, X., Roberts, E., & Dai, M. (2020). Dynamics of dissolved inorganic carbon in the South China sea: A modeling study. *Progress in Oceanography*, *186*, 102367. https://doi.org/10.1016/j.pocean.2020.102367

Du, C., Liu, Z., Dai, M., Kao, S. J., Cao, Z., Zhang, Y., et al. (2013). Impact of the Kuroshio intrusion on the nutrient inventory in the upper northern south China sea: Insights from an isopycnal mixing model. *Biogeosciences*, *10*(10), 6419–6432. https://doi.org/10.5194/bg-10-6419-2013

Duan, S. W., Liang, T., Zhang, S., Wang, L. J., Zhang, X. M., & Chen, X. B. (2008). Seasonal changes in nitrogen and phosphorus transport in the lower Changjiang River before the construction of the Three Gorges Dam. *Estuarine, Coastal and Shelf Science*, *79*(2), 239–250. https://doi.org/10.1016/j.ecss.2008.04.002

Egbert, G. D., Bennett, A. F., & Foreman, M. G. G. (1994). Topex/Poseidon tides estimated using a global inverse model. *Journal of Geophysical Research*, *99*(C12), 24821–24852. https://doi.org/10.1029/94JC01894

Eppley, R. W. (1972). Temperature and phytoplankton growth in sea. *Fishery Bulletin*, *70*(4), 1063–1085.

Fairall, C. W., Bradley, E. F., Hare, J. E., Grachev, A. A., & Edson, J. B. (2003). Bulk parameterization of air-sea fluxes: Updates and verification for the COARE algorithm. *Journal of Climate*, *16*(4), 571–591. https://doi.org/10.1175/1520-0442(2003)016<0571:BPOASF>2.0.CO;2

Gan, J., & Allen, J. S. (2002). A modeling study of shelf circulation off northern California in the region of the Coastal Ocean Dynamics Experiment: Response to relaxation of upwelling winds. *Journal of Geophysical Research*, *107*(C11), 3184–3290. https://doi.org/10.1029/2001JC001190

Gan, J., Cheung, A., Guo, X. G., & Li, L. (2009). Intensified upwelling over a widened shelf in the northeastern South China Sea. *Journal of Geophysical Research*, *114*, C09019. https://doi.org/10.1029/2007JC004660

Gan, J., Ho, H. S., & Liang, L. L. (2013). Dynamics of intensified downwelling circulation over a widened shelf in the Northeastern South China Sea. *Journal of Physical Oceanography*, *43*(1), 80–94. https://doi.org/10.1175/Jpo-D-12-02.1

Gan, J., Kung, H., Cai, Z., Liu, Z., Hui, C., & Li, J. (2022). Hotspots of the Stokes rotating circulation in a large marginal sea. *Nature Communications*, *13*(1), 2223. https://doi.org/10.1038/s41467-022-29610-z

Gan, J., Li, H., Curchitser, E. N., & Haidvogel, D. B. (2006). Modeling South China sea circulation: Response to seasonal forcing regimes. *Journal of Geophysical Research*, *111*, C06034. https://doi.org/10.1029/2005JC003298

Gan, J., Liu, Z. Q., & Hui, C. R. (2016). A three-layer alternating spinning circulation in the South China sea. *Journal of Physical Oceanography*, *46*(8), 2309–2315. https://doi.org/10.1175/JPO-D-16-0044.1

Gan, J., Liu, Z. Q., & Liang, L. L. (2016). Numerical modeling of intrinsically and extrinsically forced seasonal circulation in the China seas: A kinematics study. *Journal of Geophysical Research: Oceans*, *121*, 4697–4715. https://doi.org/10.1002/2016JC011800

Gan, J., Li, L., Wang, D. X., & Guo, X. G. (2009). Interaction of a river plume with coastal upwelling in the northeastern South China Sea. *Continental Shelf Research*, *29*(4), 728–740. https://doi.org/10.1016/j.csr.2008.12.002

Gan, J., Lu, Z., Cheung, A., Dai, M., Liang, L. L., Harrison, P. J., & Zhao, X. Z. (2014). Assessing ecosystem response to phosphorus and nitrogen limitation in the Pearl River plume using the Regional Ocean Modeling System (ROMS). *Journal of Geophysical Research: Oceans*, *119*, 8858–8877. https://doi.org/10.1002/2014JC009951

Gan, J., Lu, Z., Dai, M., Cheung, A., Harrison, P., & Liu, H. B. (2010). Biological response to intensified upwelling and to a river plume in the northeastern south China sea: A modeling study. *Journal of Geophysical Research*, *115*, C09001. https://doi.org/10.1029/2009JC005569

Gan, J., & Qu, T. (2008). Coastal jet separation and associated flow variability in the southwest South China Sea. *Deep Sea Research Part I*, *55*(1), 1–19. https://doi.org/10.1016/j.dsr.2007.09.008

Garrett, C., Maccready, P., & Rhines, P. (1993). Boundary mixing and arrested Ekman layers—Rotating stratified flow near a sloping boundary. *Annual Review of Fluid Mechanics*, *25*(1), 291–323. https://doi.org/10.1146/annurev.fl.25.010193.001451

Gong, G. C., Liu, K. K., Liu, C. T., & Pai, S. C. (1992). The chemical hydrography of the South China sea west of Luzon and a comparison with the west Philippine sea. *Terrestrial, Atmospheric and Oceanic Sciences*, *3*(4), 587–602. https://doi.org/10.3319/tao.1992.3.4.587(o)

Gordon, A. L., Orsi, A. H., Muench, R., Huber, B. A., Zambianchi, E., & Visbeck, M. (2009). Western Ross Sea continental slope gravity currents. *Deep Sea Research Part II*, *56*(13–14), 796–817. https://doi.org/10.1016/j.dsr2.2008.10.037

Gordon, A. L., Padman, L., & Bergamasco, A. (2009). Southern Ocean shelf slope exchange. Preface. *Deep Sea Research Part I*, *56*(13–14), 775–777. https://doi.org/10.1016/j.dsr2.2008.11.002

Gordon, A. L., Zambianchi, E., Orsi, A., Visbeck, M., Giulivi, C. F., Whitworth, T., & Spezie, G. (2004). Energetic plumes over the Western Ross Sea continental slope. *Geophysical Research Letters*, *31*,L21302. https://doi.org/10.1029/2004GL020785

Guo, L., Xiu, P., Chai, F., Xue, H., Wang, D., & Sun, J. (2017). Enhanced chlorophyll concentrations induced by Kuroshio intrusion fronts in the northern south China sea. *Geophysical Research Letters*, *44*, 11565–11572. https://doi.org/10.1002/2017GL075336

Heywood, K. J., Schmidtko, S., Heuze, C., Kaiser, J., Jickells, T. D., Queste, B. Y., et al. (2014). Ocean processes at the Antarctic continental slope. *Philosophical Transactions of the Royal Society A*, *372*(2019), 20130047. https://doi.org/10.1098/rsta.2013.0047

Hill, A. E. (1995). Leakage of barotropic slope currents onto the Continental Shelf. *Journal of Physical Oceanography*, *25*(7), 1617–1621. https://doi.org/10.1175/1520-0485(1995)025<1617:LOBSCO>2.0.CO;2

Li, J., & Gan, J. (2020). On the formation dynamics of the north equatorial undercurrent. *Journal of Physical Oceanography*, *50*(5), 1399–1415. https://doi.org/10.1175/JPO-D-19-0142.1

Li, Q. P., Dong, Y., & Wang, Y. (2015). Phytoplankton dynamics driven by vertical nutrient fluxes during the spring inter-monsoon period in the northeastern South China Sea. *Biogeosciences Discussions*, *12*(9), 6723–6755. https://doi.org/10.5194/bgd-12-6723-2015

Liu, K. K., Tseng, C. M., Wu, C. R., & Lin, I. I. (2010). *Carbon and nutrient fluxes in continental margins: A global synthesis*. Springer.

Liu, Z., & Gan, J. (2016). Open boundary conditions for tidally and subtidally forced circulation in a limited-area coastal model using the Regional Ocean Modeling System (ROMS). *Journal of Geophysical Research: Oceans*, *121*, 6184–6203. https://doi.org/10.1002/2016JC011975

Lu, Z., Gan, J., Dai, M., & Cheung, A. (2010). The influence of coastal upwelling and a river plume on the subsurface chlorophyll maximum over the shelf of the northeastern South China Sea. *Journal of Marine Systems*, *82*(1–2), 35–46. https://doi.org/10.1016/j.jmarsys.2010.03.002

Lu, Z., Gan, J., Dai, M., Liu, H., & Zhao, X. (2018). Joint effects of extrinsic biophysical fluxes and intrinsic hydrodynamics on the formation of hypoxia west off the Pearl River estuary. *Journal of Geophysical Research: Oceans*, *123*, 6241–6259. https://doi.org/10.1029/2018JC014199

Lu, Z., Gan, J. P., Dai, M., Zhao, X., & Hui, C. R. (2020). Nutrient transport and dynamics in the South China sea: A modeling study. *Progress in Oceanography*, *183*, 102308. https://doi.org/10.1016/j.pocean.2020.102308

Mao, M., & Xia, M. (2020). Particle dynamics in the nearshore of lake Michigan revealed by an observation-modeling System. *Journal of Geophysical Research: Oceans*, *125*, e2019JC015765. https://doi.org/10.1029/2019JC015765

Meybeck, M. (1982). Carbon, nitrogen, and phosphorus transport by world rivers. *American Journal of Science*, *282*(4), 401–450. https://doi.org/10.2475/ajs.282.4.401

Mizobata, K., Wang, J., & Saitoh, S. I. (2006). Eddy-induced cross-slope exchange maintaining summer high productivity of the Bering Sea shelf break. *Journal of Geophysical Research*, *111*, C10017. https://doi.org/10.1029/2005JC003335

Mou, L., Niu, Q., & Xia, M. (2022). The roles of wind and baroclinic processes in cross-isobath water exchange within the Bohai Sea. *Estuarine, Coastal and Shelf Science*, *274*, 107944. https://doi.org/10.1016/j.ecss.2022.107944

NASA Goddard Space Flight Center, Ocean Ecology Laboratory, Ocean Biology Processing Group. (2018). Moderate-resolution Imaging Spectroradiometer (MODIS) Aqua Chlorophyll Data; 2018 Reprocessing [Dataset]. NASA OB.DAAC. https://doi.org/10.5067/AQUA/MODIS/L3M/CHL/2018

Noble, M. A., & Ramp, S. R. (2000). Subtidal currents over the central California slope: Evidence for offshore veering of the undercurrent and for direct, wind-driven slope currents. *Deep Sea Research Part I*, *47*(5–6), 871–906. https://doi.org/10.1016/s0967-0645(99)00130-7

Olson, R. J. (1981). Differential photoinhibition of marine nitrifying bacteria—A possible mechanism for the formation of the primary nitrite maximum. *Journal of Marine Research*, *39*(2), 227–238.

Qu, T. D. (2000). Upper-layer circulation in the South China sea. *Journal of Physical Oceanography*, *30*(6), 1450–1460. https://doi.org/10.1175/1520-0485(2000)030<1450:ULCITS>2.0.CO;2

Qu, T. D. (2001). Role of ocean dynamics in determining the mean seasonal cycle of the South China Sea surface temperature. *Journal of Geophysical Research*, *106*(C4), 6943–6955. https://doi.org/10.1029/2000JC000479

Qu, T. D., Du, Y., Gan, J., & Wang, D. X. (2007). Mean seasonal cycle of isothermal depth in the South China Sea. *Journal of Geophysical Research*, *112*, C02020. https://doi.org/10.1029/2006JC003583

Qu, T. D., Girton, J. B., & Whitehead, J. A. (2006). Deepwater overflow through Luzon Strait. *Journal of Geophysical Research*, *111*, C01002. https://doi.org/10.1029/2005JC003139

Qu, T. D., Song, Y. T., & Yamagata, T. (2009). An introduction to the South China Sea throughflow: Its dynamics, variability, and application for climate. *Dynamics of Atmospheres and Oceans*, *47*(1–3), 3–14. https://doi.org/10.1016/j.dynatmoce.2008.05.001

Sasaki, Y. N., Minobe, S., Schneider, N., Kagimoto, T., Nonaka, M., & Sasaki, H. (2008). Decadal sea level variability in the South Pacific in a global eddy-resolving ocean model hindcast. *Journal of Physical Oceanography*, *38*(8), 1731–1747. https://doi.org/10.1175/2007jpo3915.1

SeaWiFS Mission page. (2019). NASA Ocean Biology Processing Group [Dataset]. NASA. https://doi.org/10.5067/ORBVIEW-2/SEAWIFS/L2/OC/2018

Shchepetkin, A. F., & McWilliams, J. C. (2005). The regional oceanic modeling system (ROMS): A split-explicit, free-surface, topography-following-coordinate oceanic model [Software]. Ocean Modelling, *9*(4), 347–404. https://doi.org/10.1016/j.ocemod.2004.08.002

Thompson, A. F., Heywood, K. J., Schmidtko, S., & Stewart, A. L. (2014). Eddy transport as a key component of the Antarctic overturning circulation. *Nature Geoscience*, *7*(12), 879–884. https://doi.org/10.1038/ngeo2289

Wong, G. T. F., Chung, S. W., Shiah, F. K., Chen, C. C., Wen, L. S., & Liu, K. K. (2002). Nitrate anomaly in the upper nutricline in the northern South China Sea - evidence for nitrogen fixation. *Geophysical Research Letters*, *29*, 2097–2112. https://doi.org/10.1029/2002GL015796

Wong, G. T. F., Pan, X. J., Li, K. Y., Shiah, F. K., Ho, T. Y., & Guo, X. H. (2015). Hydrography and nutrient dynamics in the northern south China sea shelf-sea (NoSoCS). *Deep Sea Research Part I.*, *117*, 23–40. https://doi.org/10.1016/j.dsr2.2015.02.023

Wong, G. T. F., Tseng, C. M., Wen, L. S., & Chung, S. W. (2007). Nutrient dynamics and N-anomaly at the SEATS station. *Deep Sea Research Part II*, *54*(14–15), 1528–1545. https://doi.org/10.1016/j.dsr2.2007.05.011

Wu, J. F., Chung, S. W., Wen, L. S., Liu, K. K., Chen, Y. L. L., Chen, H. Y., & Karl, D. M. (2003). Dissolved inorganic phosphorus, dissolved iron, and Trichodesmium in the oligotrophic South China Sea. *Global Biogeochemical Cycles*, *17*(1), 1008. https://doi.org/10.1029/2002GB001924

Zhou, K. B., Dai, M. H., Kao, S. J., Wang, L., Xiu, P., Chai, F., et al. (2013). Apparent enhancement of Th-234-based particle export associated with anticyclonic eddies. *Earth and Planetary Science Letters*, *381*, 198–209. https://doi.org/10.1016/j.epsl.2013.07.039